

¹ Drought indices of water demand and supply, soil moisture, vegetation, and
² their impact on LULCC in continental Chile

³ Francisco Zambrano^{a,1,*}

^a Universidad Mayor, Hémera Centro de Observación de la Tierra, Facultad de Ciencias, Escuela de Ingeniería en Medio Ambiente y Sustentabilidad, Santiago, Chile, 7500994

⁴ **Abstract**

Central Chile has been the focus of research studies due to the persistent decrease in water supply, which is impacting the hydrological system and vegetation development. This persistent period of water scarcity has been defined as a “Mega Drought”. Our objective is to examine the effects of drought on LULCC (land use land cover change) over continental Chile using drought indices of water supply and demand, soil moisture, and vegetation productivity. For the analysis, continental Chile was divided into five zones according to a latitudinal gradient: “Norte Grande,” “Norte Chico,” “Centro,” “Sur,” and “Austral.” The monthly ERA5-Land (ERA5L) variables for precipitation, temperature, and soil moisture were used. From 2001 to 2022, we used the land cover MODIS product MCD12Q1, and from 2000 to 2023, we used the NDVI (Normalized Difference Vegetation Index) product MOD13A3 collection 6.1. We estimated atmospheric evaporative demand (AED) using the Hargreaves-Samani equation with the ERA5L temperature. We used the Standardized Precipitation Index (SPI), the Standardized Precipitation Evapotranspiration Index (SPEI), the Evaporative Demand Drought Index (EDDI), the Standardized Soil Moisture Index (SSI), and the Standardized anomaly of cumulative NDVI (zcNDVI) as drought indicators. These indices were calculated for time scales of 1, 3, 6, 12, 24, and 36 months, except for zcNDVI, which was for 6 months. We analyze the trend for LULCC, vegetation productivity, and drought indices. Also, we analyzed the temporal correlation of SPI, SPEI, EDDI, and SSI with zcNDVI to gain insights into the impact of water supply and demand on vegetation productivity. Our results showed that LULCC were highest in “Centro,” “Sur,” and “Austral,” with 36%, 31%, and 34%, respectively. The EDDI shows that water demand has increased for all zones, with a major increase in “Norte Grande.” The drought indices of water supply and soil moisture evidence a decreasing trend, which decreases at longer time scales, from “Norte Grande” to “Sur.” “Austral” is the only zone that shows an increase in supply. Vegetation productivity measures by zcNDVI present a negative trend in “Norte Chico” and “Centro.” Showing to be the zones most impacted by climatic conditions, the years 2020 and 2022 suffered the most extreme drought. On the other hand, forests seem to be the most resistant to drought. The types that show to be most affected by variation in climate conditions are shrublands, savannas, and croplands. The drought indices that have the capability of explaining to a major degree the variance in vegetation productivity are SSI-12, followed by SPEI-24 and SPEI-12 in “Norte Chico” and “Centro.” The results indicate that “Norte Chico” and “Zona Central” are the most sensitive regions to water supply deficits longer than a year, potentially explained by a low capacity of water storage in those zones that should be further investigated.

⁵ **Keywords:** drought, land cover change, satellite

*Corresponding author

Email address: francisco.zambrano@umayor.cl (Francisco Zambrano)

¹This is the first author footnote.

6 **1. Introduction**

7 The sixth assessment report (AR6) of the IPCC (Calvin et al., 2023) indicates that human-induced green-
8 house gas emissions have increased the frequency and/or intensity of some weather and climate extremes,
9 and the evidence has been strengthened since AR5 (IPCC, 2013). There is a high degree of confidence
10 that rising temperatures will increase the land area where droughts will occur more frequently and with
11 greater severity (Seneviratne, 2021). Furthermore, drought increases tree mortality and triggers changes in
12 land cover and, consequently, land use, thus impacting ecosystems (Crausbay et al., 2017). Nevertheless,
13 there is a lack of understanding of how the alteration in water supply and demand is affecting land cover
14 transformations.

15 The primary cause of drought is precipitation, and temperature makes it worse (Luo et al., 2017). Drought
16 impacts soil moisture, hydrological regimes, and vegetation productivity. Initially, drought was commonly
17 classified as meteorological, hydrological, and agricultural (Wilhite and Glantz, 1985). Lately, Van Loon
18 et al. (2016) and AghaKouchak et al. (2021) have given an updated definition of drought for the Anthro-
19 pocene, suggesting that it should be considered the feedback of humans' decisions and activities that drives
20 the anthropogenic drought. Even though it has been argued that those definitions do not fully address
21 the ecological dimensions of drought, Crausbay et al. (2017) proposed the ecological drought definition as
22 "an episodic deficit in water availability that drives ecosystems beyond thresholds of vulnerability, impacts
23 ecosystem services, and triggers feedback in natural and/or human systems." Moreover, many ecological
24 studies have misinterpreted how to characterize drought, for example, sometimes considering "dry" condi-
25 tions as "drought" (Slette et al., 2019). On the other hand, the AR6 (Calvin et al., 2023) predicts that many
26 regions of the world will experience more severe agricultural and ecological droughts even if global warming
27 stabilizes at 1.5°–2°C. Then, there is a challenge in conducting drought research, especially to evaluate its
28 impact on ecosystems.

29 Chile has been facing a persistent rainfall deficit for more than a decade (Garreaud et al., 2017), which
30 has impacted vegetation development (Zambrano, 2023) and the hydrological system (Boisier et al., 2018).
31 Current drought conditions have affected crop productivity (Zambrano et al., 2016, 2018), forest development
32 (Miranda et al., 2020; Venegas-González et al., 2018), forest fire occurrence (Urrutia-Jalabert et al., 2018),
33 land cover change (Fuentes et al., 2021), water supply in watersheds (Alvarez-Garreton et al., 2021), and
34 have had economic impacts (Fernández et al., 2023). In 2019–2020, the drought severity reached an extreme
35 condition in Central Chile (30–34°S) not seen for at least 40 years, and the evidence indicates that the
36 impact is transversal to the land cover classes of forest, grassland, and cropland (Zambrano, 2023). The
37 prolonged lack of precipitation in Central Chile is producing changes in ecosystem dynamics that must be
38 studied.

39 For the spatiotemporal assessment of drought impact (i.e., by water supply and demand) on land cover
40 changes, we need climatic reliable variables such as precipitation, temperature, soil moisture, land cover, and
41 vegetation status. For developing countries like Chile, the weather networks present several disadvantages,
42 such as gaps, a short history, and low-quality data. Reanalysis data, as the ERA5-Land (ERA5L) (Muñoz-
43 Sabater et al., 2021) provides hourly climatic information (precipitation, temperature, and soil moisture)
44 without gaps since 1950 with global extension. ERA5L has already been used for drought assessment using
45 the Standardized Precipitation-Evapotranspiration Index (SPEI) (Nouri, 2023) and for flash drought (Wang
46 et al., 2023) by analyzing soil moisture and evapotranspiration. On the other hand, satellite remote sensing
47 (West et al., 2019; AghaKouchak et al., 2015) is the primary method to evaluate how drought impacts
48 vegetation dynamics. The Moderate-Resolution Imaging Spectroradiometer (MODIS) can be used to get
49 vegetation drought indices (VDI), which are often used as proxies for productivity (Paruelo et al., 2016;
50 Schucknecht et al., 2017). Besides, land use and land cover (LULC) change can be driven by drought (Tran
51 et al., 2019; Akinyemi, 2021). To analyze these changes, multiple LULC products exist (Grekousis et al.,
52 2015). One of those that provides time series since 2001 is the MCD12Q1 (Friedl and Sulla-Menashe, 2019)
53 from MODIS. The variation in water supply and demand is finally reflected in the total water storage
54 (TWS). The Gravity Recovery and Climate Experiment (GRACE), which allows analyzing changes in water

55 availability at coarse resolution, can retrieve the TWS (Ahmed et al., 2014; Ma et al., 2017). We can
56 find drought indices of supply (i.e., precipitation) and demand (i.e., temperature) using climatic reanalysis
57 (ERA5L) and vegetation data (MODIS). This lets us figure out how drought changes LULC. Further, the
58 TWS can be assessed with regard to the changes in water supply and demand to gain insight into the impact
59 on water storage.

60 To evaluate meteorological drought (i.e., water supply), the World Meteorological Organization (WMO;
61 WMO et al. (2012)) recommends the Standardized Precipitation Index (SPI; McKee et al. (1993)), a multi-
62 scalar drought index that allows to monitor precipitation deficits from short- to long-term. Following the
63 same approach, Vicente-Serrano et al. (2010) incorporates into the SPI the effect of temperature through
64 the use of potential evapotranspiration, thus proposing the SPEI (Standardized Precipitation Evapotranspi-
65 ration Index). Similarly, to evaluate solely the evaporative demand driven by temperature, Hobbins et al.
66 (2016) and McEvoy et al. (2016) came up with the Evaporative Demand Drought Index (EDDI). For veg-
67 etation, in a similar manner as the SPI, SPEI and EDDI; Zambrano et al. (2018) proposed the zcNDVI,
68 a standardized anomaly of the cumulative Normalized Difference Vegetation Index (NDVI), which could
69 be accumulated over the growing season or any period (e.g., months), resulting in a multiscalar drought
70 index. For soil moisture, several drought indices exist, such as the Soil Moisture Deficit Index (SDMI) a
71 normalized index (Narasimhan and Srinivasan, 2005) and the Soil Moisture Agricultural Drought Index
72 (SMADI) (Souza et al., 2021) which is a normalized index using vegetation, land surface temperature, and a
73 vegetation condition index (VCI, (Kogan, 1995)). From TWS, we can estimate the standardized terrestrial
74 water storage index (STI) (Cui et al., 2021), a standardized anomaly that follows the methodology of the
75 SPI, SPEI, EDDI, and zcNDVI. Thereby, we have drought indices for water supply, demand, and storage,
76 which can help to make a comprehensive assessment of drought.

77 In this research, we aim to analyze the impact of drought on different types of ecosystems (land cover
78 classes) in continental Chile. Our specific goals are: i) to analyze the trend on multi-scalar drought indices
79 for water demand and supply, soil moisture, and vegetation productivity for 1981–2023/2001–2023; ii) to
80 assess the LULC change for 2001–2021 and how it relates to drought indices; iii) to evaluate the relationship
81 between zcNDVI, a measure of vegetation productivity, and drought indices for water demand and supply
82 and soil moisture; and iv) to assess if the observed changes in the drought indices are linked to TWS.

83 2. Study area

84 Continetal Chile has a diverse climate condition from north to south and east to west (Aceituno et al.,
85 2021) (Figure 1), which determines its great ecosystem diversity (Figure 2). The Andes Mountains are a
86 main factor in latitudinal variation (Garreaud, 2009). To describe the climate and ecosystem of Chile, we
87 use the Koppen-Geiger release by Beck et al. (2023) and the land cover type persistance of 80% of times
88 for 2001–2022, from the IGBP classification scheme (Friedl and Sulla-Menashe, 2019) (see Section 3.4).
89 “Norte Grande” and “Norte Chico” predominate in an arid desert climate with hot (Bwh) and cold (Bwk)
90 temperatures. At the south of “Norte Chico,” the climate changes to an arid steppe with cold temperatures
91 (Bsk). Mainly, the land is barren, with a minor surface of vegetation types such as shrubland and grassland.
92 In the zones “Centro” and the north half of “Sur,” the main climate is Mediterranean, with warmer to hot
93 summers (Csa and Csb). There is a significant amount (50%) of Chilean matorral (shrubland and savanna,
94 (Fuentes et al., 2021)), then grassland (16%), forest (8%), and croplands (5%), in “Centro.” The south part
95 of “Sur” and the north part of “Austral” are dominated by an oceanic climate (Cfb). Those zones are high
96 in forest and grassland. The southern part of the country has a tundra climate, and in Patagonia, it is a
97 cold semi-arid area with an extended surface of grassland, forest, and, to a lesser extent, savanna.

98 3. Materials and Methods

99 3.1. Software and packages used

100 For the downloading, processing, and analysis of the spatio-temporal data, we used the open source software
101 for statistical computing and graphics, R (R Core Team, 2023). For downloading ERA5L, we used the

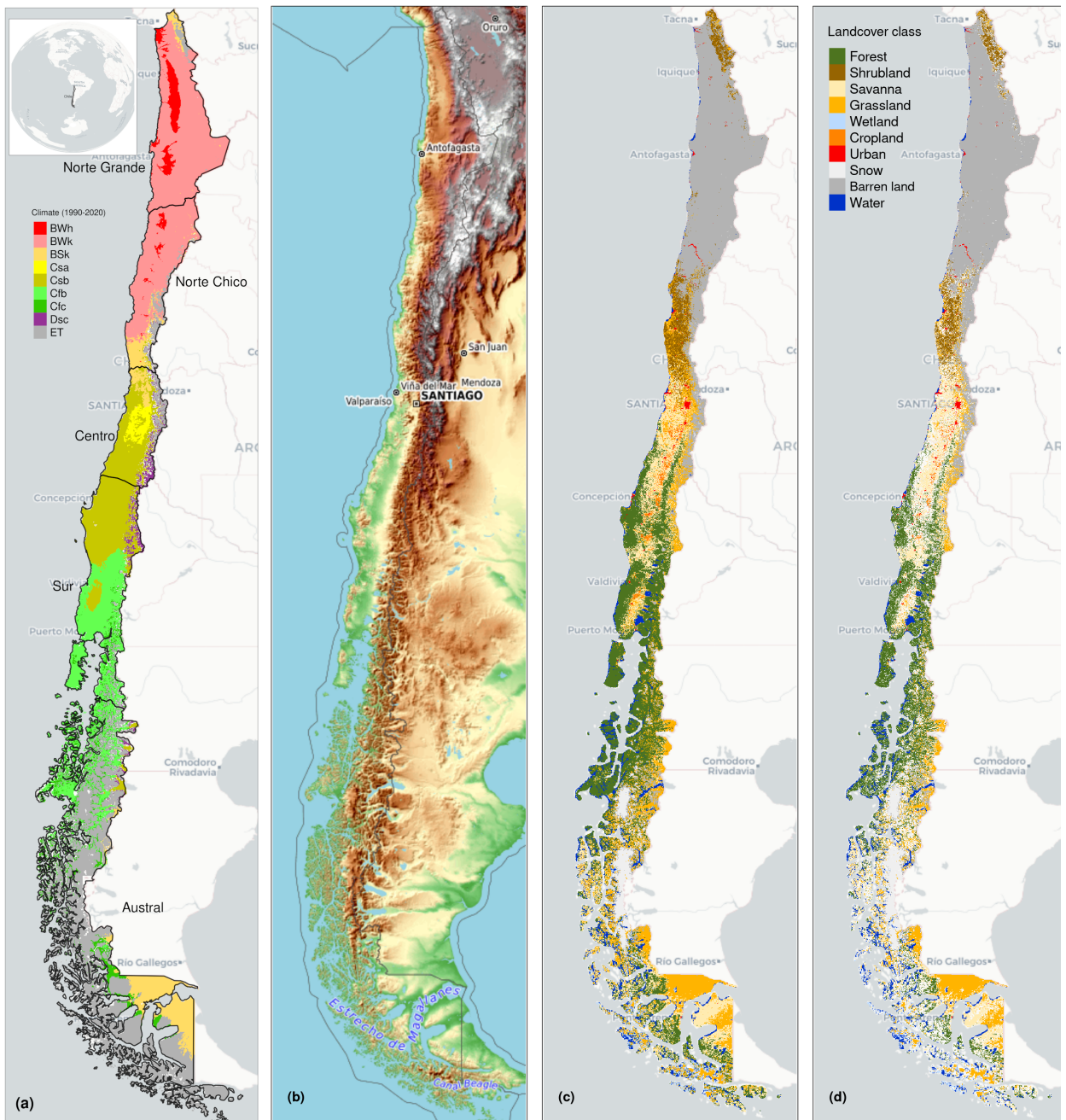


Figure 1: (a) Chile with the Koppen-Geiger climate classes and the five macrozones “Norte Grande”, “Norte Chico”, “Centro”, “Sur”, and “Austral”. (b) Topography reference map. (c) Land cover classes for 2022. (d) Persistent land cover classes (> 80%) for 2001-2022

102 {ecmwfr} package (Hufkens et al., 2019). For processing raster data, we used {terra} (Hijmans, 2023) and
 103 {stars} (Pebesma and Bivand, 2023). For managing vectorial data, we used {sf} (Pebesma, 2018). For
 104 the calculation of AED, we used {SPEI} (Beguería and Vicente-Serrano, 2023).

105 *3.2. Data*

106 *3.2.1. Earth observation data*

107 For water supply and demand variables, we used ERA5L ([Muñoz-Sabater et al., 2021](#)), a reanalysis dataset
108 that provides the evolution of land variables since 1950. It has a spatial resolution of 0.1° , hourly frequency,
109 and global coverage. We selected the variables for total precipitation, 2 meter temperature maximum and
110 minimum, and volumetric soil water layers between 0 and 100cm of depth (layer 1 to layer 3). The data
111 was downloaded using the Copernicus Climate Data Store (CDS) Application Program Interface (API)
112 implemented in `{ecmwf}` ([Hufkens et al., 2019](#)).

113 To derive a proxy of vegetation productivity, we used the product MOD13A3 collection 6.1 from MODIS
114 ([Didan, 2015](#)). It provides vegetation indices (NDVI and EVI) at 1km of spatial resolution and monthly
115 frequency. The MOD13A3.061 and MCD12Q1.061 were retrieved from the online Data Pool, courtesy of
116 the NASA EOSDIS Land Processes Distributed Active Archive Center (LP DAAC), USGS Earth Resources
117 Observation and Science (EROS) Center, Sioux Falls, South Dakota, <https://lpdaac.usgs.gov/tools/data-pool/>.

Table 1: Description of the earth observation data used

Product	Sub-product	Variable	Spatial Resolution	Period	Units	Short Name
ERA5L		Precipitation	0.1°	1981-2023	mm	P
		Maximum temperature			$^\circ C$	T_{max}
		Minimum temperature			$^\circ C$	T_{min}
		Volumetric Soil Water Content at 1m			m^3/m^3	SM
ERA5L*	MOD13A3.061	Atmospheric Evaporative Demand	0.1°	1981-2023	mm	AED
MODIS		Normalized Difference Vegetation Index	1 km	2000-2023		NDVI
		land cover IGBP scheme		2001-2022		land cover

*Derived from ERA5L with Eq. 1.

119 *3.2.2. in-situ data*

120 POR COMPLETAR

121 *3.2.3. Validation of ERA5L variables*

122 POR COMPLETAR

123 *3.3. Drought Indices*

124 *3.3.1. Atmospheric Evaporative Demand (AED)*

125 For the indices EDDI and SPEI that use water demand, first we have to calculate the AED. For this, we
126 used the method of Hargreaves ([Hargreaves, 1994; Hargreaves and Samani, 1985](#)):

$$AED = 0.0023 \cdot Ra \cdot (T + 17.8) \cdot (T_{max} - T_{min})^{0.5} \quad (1)$$

127 where Ra ($MJ m^2 day^{-1}$) is extraterrestrial radiation; T , T_{max} , and T_{min} are mean, maximum, and
128 minimum temperature ($^\circ C$). We calculate the centroid coordinates per pixel and use the latitude to estimate
129 Ra .

130 We chose the method of Hargreaves to estimate AED because of its simplicity, which only requires tem-
131 peratures and extrarrestrial radiation. Also, it has been recommended over other methods when the use of
132 several climatic variables is limited ([Vicente-Serrano et al., 2014](#)).

133 3.3.2. Non-parametric calculation of drought indices

134 We derived the drought indices of water supply and demand, soil moisture from the ERA5L dataset, and
 135 vegetation from the MODIS product, all at monthly frequency.

136 To evaluate water demand, we chose the *EDDI* (Hobbs et al., 2016; McEvoy et al., 2016) index, which
 137 uses the *AED*. For supply, we used the index recommended by the World Meteorological Organization
 138 (WMO) for monitoring drought, the *SPI* (McKee et al., 1993). We calculated the *SPEI*, which used a
 139 balance between *P* and *AED*, in this case, an auxiliary variable *D* = *P* – *AED* is used. In this study,
 140 we used the *SSI* (standardized soil moisture index at 1 m) (Hao and AghaKouchak, 2013; AghaKouchak,
 141 2014), which uses soil moisture at 1m depth. Finally, for the proxy of productivity, *zcNDVI*, we used the
 142 *NDVI*. Before using the *NDVI*, it was smoothed using a locally-weighted polynomial regression, following
 143 the procedure described in Zambrano et al. (2018) and Zambrano et al. (2016).

144 All the indices are multi-scalar and were calculated for time scales of 1, 3, 6, 12, 24, and 36 months, except
 145 for *zcNDVI*, which was calculated for 6 months. The goal is to be able to evaluate short- and long-term
 146 droughts in water demand and supply and soil moisture. This is particularly important for central Chile
 147 because it has suffered from a prolonged decrease in precipitation for more than 12 years (Garreaud et al.,
 148 2020; Boisier et al., 2018; Garreaud et al., 2017).

149 To calculate the drought indices, first we must calculate the accumulation of the variable. In this case, for
 150 generalization purposes, we will use *V*, referring to *P*, *AED*, *D*, *NDVI*, and *SM* (Table 1). We cumulated
 151 each *V* over the time series of *n* values, and for the time scales *s*:

$$A_{si} = \sum_{i=n-s-i+2}^{n-i+1} V_i \quad \forall i \geq n - s + 1 \quad (2)$$

152 It corresponds to a moving window (convolution) that sums the variable for *s* starting for the last month
 153 *n* until the month, which could sum for *s* months (*n*-*s*+1). Once the variable is cumulated over time
 154 for the scale *s*, we used a nonparametric approach following Hobbs et al. (2016) to derive the drought
 155 indices. Thus, the empirically derived probabilities are obtained through an inverse normal approximation
 156 (Abramowitz and Stegun, 1968). Then, we used the empirical Tukey plotting position (Wilks, 2011) over
 157 *A_i* to derive the *P(A_i)* probabilities across a period of interest:

$$P(A_i) = \frac{i - 0.33}{n + 0.33} \quad (3)$$

158 The drought indices *SPI*, *SPEI*, *EDDI*, *SSI*, and *zcNDVI* are obtained following the inverse normal
 159 approximation:

$$DI(A_i) = W - \frac{C_0 + C_1 \cdot W + c_2 \cdot W^2}{1 + d_1 \cdot W + d_2 \cdot W^2 + d_3 \cdot W^3} \quad (4)$$

160 *DI* is referring to the drought index calculated for the variable *V*. The values for the constants are:
 161 *C₀* = 2.515517, *C₁* = 0.802853, *C₂* = 0.010328, *d₁* = 1.432788, *d₂* = 0.189269, and *d₃* = 0.001308. For
 162 *P(A) ≤ 0.5*, *W* = $\sqrt{-2 \cdot \ln(P(A_i))}$, and for *P(A_i) > 0.5*, replace *P(A_i)* with $1 - P(A_i)$ and reverse the sign
 163 of *DI(A_i)*.

164 3.4. LULC change for 2001-2022 and its relation with water supply and demand, and soil moisture

165 3.4.1. land cover macroclasses and validation

166 To analyze the LULCC, we use the IGBP scheme from the MCD12Q1 collection 6.1 from MODIS. This
 167 product has a yearly frequency from 2001 to 2022. The IGBP defines 17 classes; from these, we regrouped
 168 into ten macroclasses, as follows: classes 1-4 to forest, 5-7 to shrublands, 8-9 to savannas, 10 as grasslands,

169 11 as wetlands, 12 and 14 to croplands, 13 as urban, 15 as snow and ice, 16 as barren, and 17 to water
170 bodies. Thus, we have a land cover raster time-series with the ten classes for 2001 and 2023.

171 To validate the land cover obtained, we compare the macroclasses with the ones of a more detailed land
172 cover map made by [Zhao et al. \(2016\)](#) for Chile with samples acquired in the years 2013–2014 (LCChile).
173 The later has a spatial resolution of 30 m and three levels of defined classes; from those, we used level 1,
174 which fits with the macroclasses land cover. We chose the years 2013 (IGBP2013) and 2014 (IGBP2014)
175 from land cover macrolcasses to validate with LCChile.

176 We follow the next procedure:

- 177 i) resampled LCChile to the spatial resolution (500m) of the land cover macroclasses using the nearest
178 neighbor method,
179 ii) took a random sample of 1000 points within continental Chile and extracted the classes that fell within
180 each point for LCChile, IGBP2013, and IGBP2014; we considered the point extracted from LCChile
181 as the truth and the values as the other two years as prediction
182 iii) calculate a confusion matrix with the classes extracted in the 1000 poitns for LCChile, IGBP2013, and
183 IGBP2014. Calculate the performance metrics of accuracy and F1.

$$184 \quad Accuracy = \frac{TP + TN}{TP + TN + FP + FN} = \frac{\text{correct classifications}}{\text{all classifications}}$$
$$F1 = \frac{2 \cdot TP}{2 \cdot TP + FP + FN}$$

185 where TP and FN refer to true positive and false negative, correctly classified classes; TN and FP to true
186 negative and false positive, wrongly classified classes.

187 3.4.2. *land cover persistence mask 2001-2022*

188 The time series of NDVI is affected by climatic conditions, vegetation development, seasonality, and changes
189 in vegetation type. In this study, we want to analyze the variation in vegetation productivity in different
190 land cover types and how it is affected by water demand, water supply, and soil moisture. In order to
191 avoid changes due to a change in the land cover type, that will wrongly impact NDVI. We will develop a
192 persistence mask for land cover for 2001–2023. Thereby, we reduce an important source of variation on a
193 regional scale.

194 Thus, we calculated a raster mask for IGBP MODIS considering the macroclasses that remain without
195 change for more than 80% of the years (2001–2022) per pixel, which allows us to identify the areas with no
196 land cover change for the macroclasses.

197 3.4.3. *land cover trend and drought indices*

198 We calculated the surface occupied per land cover class into the five macrozones (“Norte Grande” to
199 “Austral”) per year for 2001–2023. After that, we calculated the trend’s change in surface; we used the Sen’
200 slope ([Sen, 1968](#)) based on Mann-Kendall ([Kendall, 1975](#)). This way, we obtain a matrix of trends of 5 x 5
201 (macrozones x land cover). The aim is to later explore if the trend in land cover classes is associated with
202 a trend in the drought indices. For this, we will use the techniques of regresion and regularization of Lasso
203 ([Tibshirani et al., 2010](#)) and Ridge ([Hoerl and Kennard, 1970](#)). Also, we will test random forests for this
204 purpose ([Ho, 1995](#)). We will choose the trend of land cover surface per macroclass and macrozone as the
205 response variable and the trend of the drought indices (SPI, SPEI, EDDI, and SSI for time scales 1, 3, 6, 12,
206 24, and 36 months) as the predictor variables. With this analysis, we expect to gather insights regarding
207 whether there is a pattern of climatic influence along Chile or if what is happening in Central Chile has to
208 do with more localized climatic conditions.

209 3.5. Trend of drought indices for water demand and supply, soil moisture, and vegetation productivity

210 3.5.1. Mann-Kendall and Sen's slope

211 To estimate if there are significant positive or negative trends for the drought indices, we used the non-
212 parametric test of Mann-Kendall (Kendall, 1975). To determine the magnitude of the trend, we used Sen's
213 slope (Sen, 1968). Some of the advantages of applying this methodology are that the Sen's slope is not
214 affected by outliers as regular regression does, and it is a non-parametric method that is not affected by the
215 distribution of the data. We applied both to the six time scales from 1981 to 2023 (monthly frequency) and
216 the indices SPI, EDDI, SPEI, and SSI. In the case of zcNDVI (six months) was for 2000 to 2023. Thus, we
217 have 31 trends. Also, we extracted the trend aggregated by macrozone and land cover class, obtaining a
218 table of 31x5x5 (drought indices trends x macrozone x land cover class). We will use this data in Section 3.4
219 to analyze if there is a strong relationship between the trends of drought indices and land cover surface
220 within continental Chile.

221 3.5.2. Trend in vegetation productivity without land cover change

222 Vicente-Serrano et al. (2022) made a global analysis of the drought's severity trend using SPI, SPEI, and
223 the Standardized Evapotranspiration Deficit Index (SEDI; Vicente-Serrano et al. (2018)) to evaluate AED.
224 They indicate that the increase in hydrological drought has been due to anthropogenic effects rather than
225 climate change. This is because the global increase in AED did not explain the change in the spatial pattern
226 of the hydrological drought. Also, they state that “*the increase in hydrological droughts has been primarily
227 observed in regions with high water demand and land cover change*”. We will contrast this hypothesis with
228 what is occurring in Chile. To achieve this, we will use the land cover class type that remains more than
229 80% of types for 2001–2022 to evaluate the trend on zcNDVI and use this as a mask where there are low
230 changes.

231 3.6. Impact for water supply and demand, and soil moisture in vegetation productivity within land cover
232 types

233 We analyze the drought indices of water demand and supply and soil moisture against vegetation to address:
234 i) if short- or long-term time scales are most important in impacting vegetation through Chile; and ii) the
235 strength of the correlation for the variable and the time scale. Then, we will summarize for each land cover
236 class and macrozone. Thus, we will be able to advance in understanding how climate is affecting vegetation,
237 considering the impact on the five macroclasses having vegetation: forest, cropland, grassland, savanna, and
238 shrubland.

239 To assess how water demand and supply and soil moisture are related to vegetation productivity (zcNDVI),
240 we analyze the linear correlation between the indices SPI, SPEI, EDDI, and SSI for 1, 3, 6, 12, 24, and
241 36-month time scales against zcNDVI. We followed a similar approach to that used by Meroni et al. (2017)
242 when using the SPI for meteorological drought against the cumulative FAPAR (Fraction of Absorbed Photo-
243 synthetically Active Radiation) as a proxy for vegetation productivity. We made a pixel-to-pixel linear
244 correlation analysis per index. First, we calculate the Pearson coefficient of correlation for the six time scales
245 and let the time scale that reaches the maximum correlation be significant ($p < 0.05$). Then, we extracted
246 the Pearson correlation value corresponding to the time scales that reached the maximum value. Thus, we
247 derived two raster maps per index, the first with the time scales and the second with the correlation value.

248 4. Results

249 4.1. Data

250 4.1.1. Validation of ERA5L variables

251 4.2. LULC change for 2001–2022 and its relation with water supply and demand, and soil moisture

252 4.2.1. land cover macroclasses and validation

253 For vegetation, we obtained and use hereafter five macroclasses of land cover from IGBP MODIS: forest,
254 shrubland, savanna, grassland, and croplands. Figure 1 c shows the spatial distribution of the macroclasses

255 through Chile for the year 2022. The validation of IGBP2013 and IGBP2014 with LCChile reached near
 256 the same metrics of performance, having an accuracy of ~0.82 and a F1 score of ~0.66 (see SS1).

257 4.2.2. land cover persistence mask 2001-2022

258 Figure 1 d, shows the macroclasses of land cover persistiance (80%) during 2021-2022, respectively. Within
 259 continental Chile, forest is the vegetation type with highest surface with $135,00 \text{ km}^2$, followed by grassland
 260 ($73,176 \text{ km}^2$), savanna ($54,410 \text{ km}^2$), shrubland ($24,959 \text{ km}^2$), and cropland ($3,100 \text{ km}^2$) (2). The macrozones
 261 with major LULCC for 2001-2022 were “Centro”, “Sur”, and “Austral” with 36%, 31%, and 34%, respectively
 262 (Figure 1 and Table 3); of its surface that changes the type of land cover. Figure 2 shows the summary
 263 of the proportion of surface per land cover class and macrozone, derived from the persistiance mask over
 264 continental Chile.

Table 2: Surface of the land cover class that persist during 2001-2022

macrozone	Surface [km^2]					
	Forest	Cropland	Grassland	Savanna	Shrubland	Barren land
Norte Grande		873		7,796	169,244	
Norte Chico	88	4,221	580	16,085	83,059	
Centro	3,685	1,876	7,475	19,420	832	12,304
Sur	71,943	1,135	7,094	15,676		2,143
Austral	59,481		53,514	18,733	245	7,114

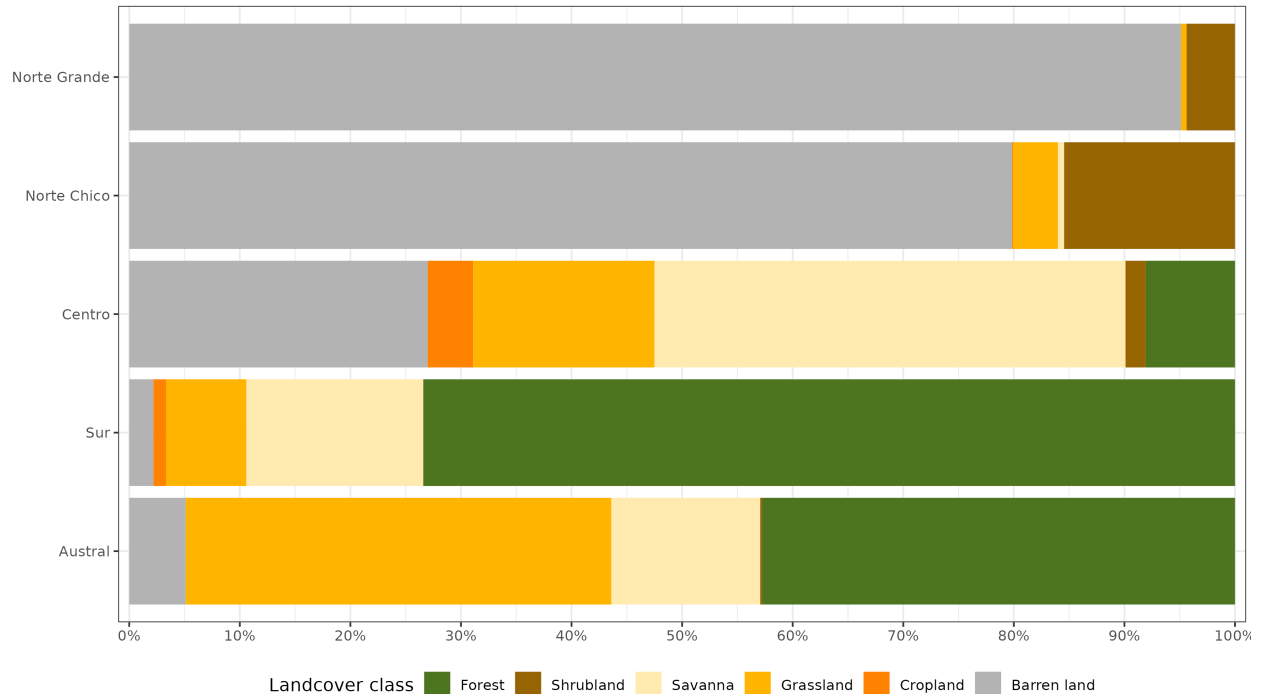


Figure 2: Proportion of land cover class from the persistent land cover for 2001-2022 (>80%) per macrozone

265 4.2.3. land cover trend and drought indices

266 The “Norte Chico” shows an increase in barrend land of $111 \text{ km}^2 \text{year}^{-1}$ and a reduction in the class
 267 savanna of $70 \text{ km}^2 \text{year}^{-1}$. In the “Centro” and “Sur,” there are changes in the Chilean matorral, with an

Table 3: The value of Sen's slope trend next to the time-series plot of surface per land cover class (IGBP MCD12Q1.016) for 2001–2022 through Central Chile. Values of zero indicate that there was not a significant trend. Red dots on the plots indicate the maximum and minimum values of surface.

macrozone	Trend of change [$\text{km}^2 \text{ year}^{-1}$]											
	Forest		Cropland		Grassland		Savanna		Shrubland		Barren land	
	x	y	x	y	x	y	x	y	x	y	x	y
Norte Grande								0.0			0.0	0.0
Norte Chico					-12.1			0.0		-70.0		111.2
Centro		0.0			-22.4		83.2		-136.2		146.0	22.9
Sur		396.6			37.8		0.0		-318.8			0.0
Austral		0.0					0.0		172.1		-36.9	-93.2

268 important reduction in savanna (136 to $318 \text{ km}^2 \text{ yr}^{-1}$), and an increase in shrubland and grassland. Showing
269 a change for more dense vegetation types. It appears to be a shift in the area of cropland from the “Centro”
270 to the “Sur.” Also, there is a high increase in forest ($397 \text{ km}^2 \text{ yr}^{-1}$) in the “Sur,” replacing the savanna lost.

271 Further, we want to address whether the trend in land cover change for 2001–2023 is associated with
272 trends in drought indices of water demand and supply and/or soil moisture for macrozone and land cover
273 macroclasses. From the three methods tested, Ridge, Lasso, and Random Forest, neither gives significant
274 results regarding whether the trend in a drought index for any time scale explains the trend in land cover
275 change. Nevertheless, in “Norte Chico” and “Centro,” there is a decrease in croplands and savanna and an
276 increase in barren land, which is associated with the variation in drought indices. Mainly for a decrease in
277 water supply (SPI and SSI) and an increase in water demand (EDDI). However, due to the high variability
278 from north to south in Chile, the climatic condition (arid, semi-arid, and humid), and the land cover type,
279 we believe that only in those zones could the LULCC be driven to some degree by drought.

280 4.3. Trend of drought indices for water demand and supply, soil moisture, and vegetation productivity

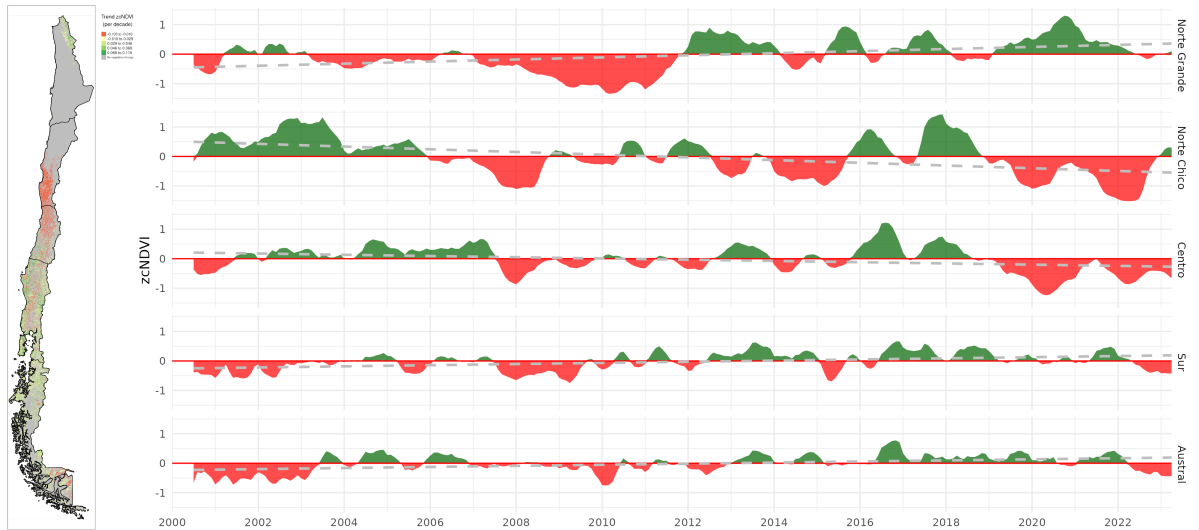


Figure 3: (a) Map of the linear trend of the index zcNDVI-6 for 2001–2023. Greener colors indicate a positive trend; redder colors correspond to a negative trend and a decrease in vegetation productivity. Grey colors indicate either no vegetation or a change in land cover type for 2001–2022. (b) Temporal variation of zcNDVI-6 aggregated at macrozone level within continental Chile. Each horizontal panel corresponds to a macrozone from ‘Norte Grande’ to ‘Austral’.

281 Regarding vegetation productivity aggregated through the macrozones in the five land cover macroclasses,
 282 in “Norte Grande,” there is an increase trend of 0.02 (z-index) per decade, related to types of grassland
 283 and shrubland. There is a negative trend in “Norte Chico” with -0.04 and “Centro” with -0.02 per decade.
 284 In the “Norte Chico,” savanna (-0.05) has the lowest trend, and the rest of the types are around -0.04. In
 285 “Centro,” shrubland reaches -0.06, grassland -0.05, and croplands and savanna -0.01 per decade. This could
 286 be associated either with a reduction in vegetation surface, a decrease in biomass, or browning ([Miranda et al., 2023](#)). Vegetation reached its lowest values since the year 2019, reaching an extreme condition in early
 287 2020 and 2022 in the “Norte Chico” and Centro” (Mega Drought). The “Sur” and “Austral” show a positive
 288 trend of around 0.016 per decade (Figure 3). Despite the croplands suffering from drought just as badly as
 289 the native vegetation in “Norte Chico,” the Chilean matorral appears to be the region most affected by a
 290 negative trend in vegetation ([Fuentes et al., 2021](#)).
 291

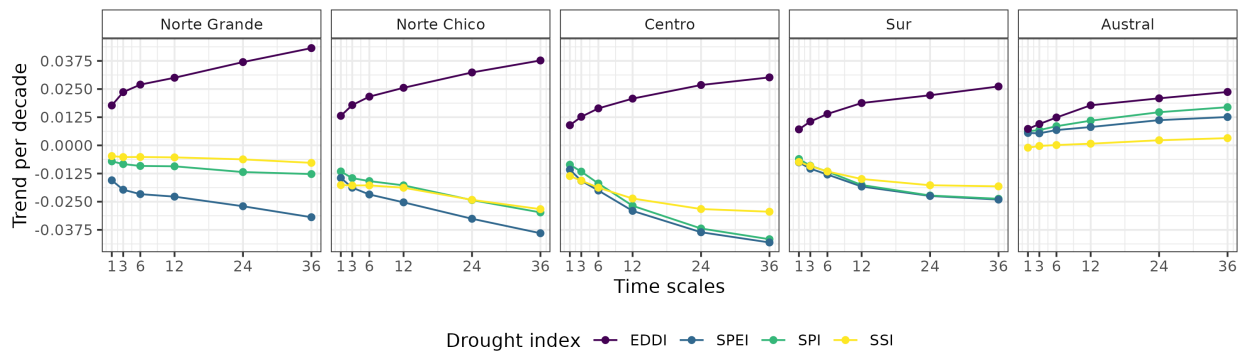
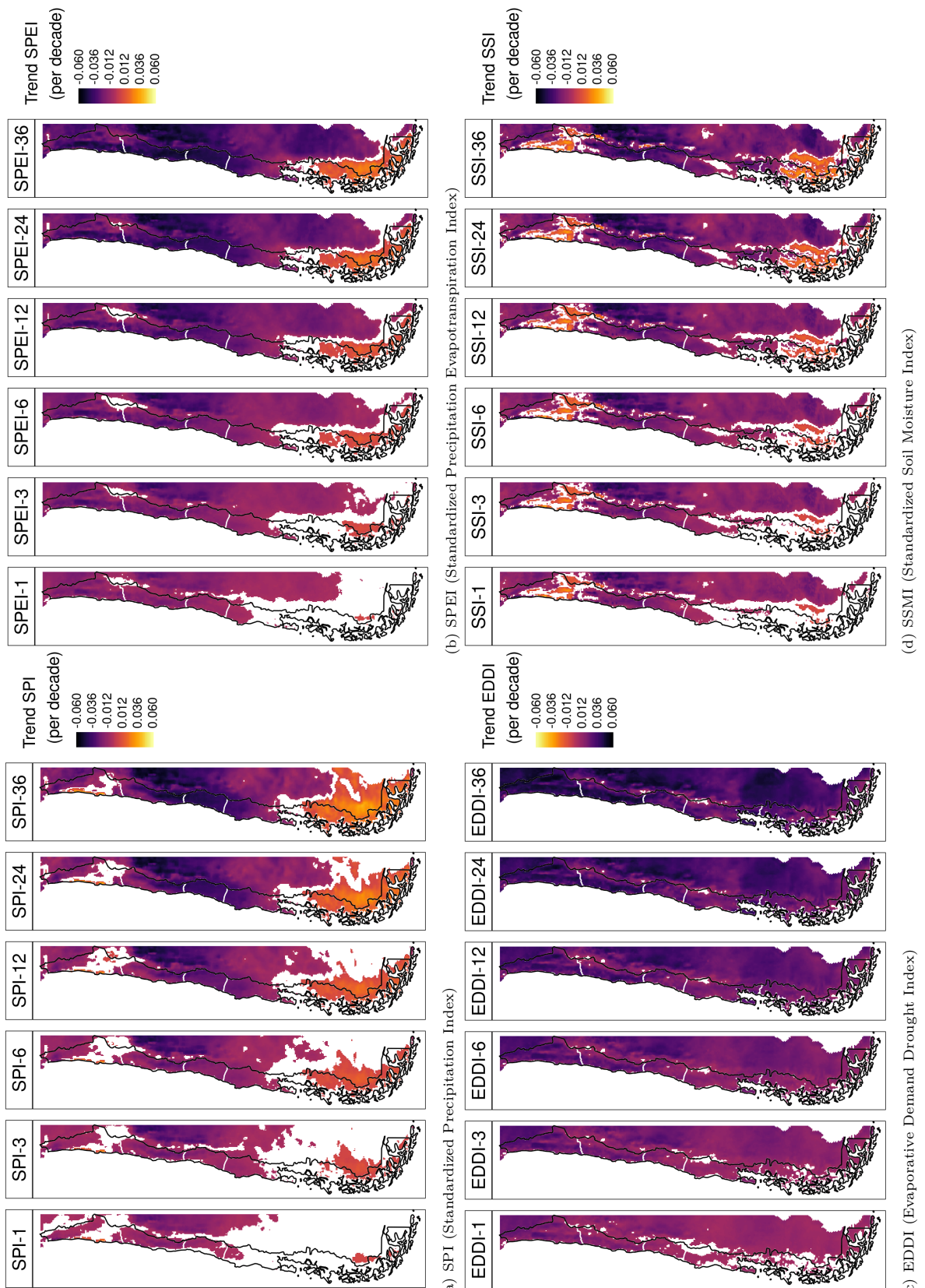


Figure 4: Trend per decade for the drought indices SPI, EDDI, SPEI, and SSI aggregated by macrozone.

292 Analyzing the water supply, the macrozones that have the lowest trend are “Norte Chico” and “Centro,”
 293 where the SPI, SPEI, and SSI show that it decreases at longer time scales due to the prolonged reduction in
 294 precipitation. At 36 months, it reaches trends between -0.03 and -0.04 (z-score) per decade for SPI, SPEI,
 295 and SSI (Figure 5). For “Sur,” the behavior is similar, decreasing at longer scales and having between -0.016
 296 and -0.025 per decade for SPI, SPEI, and SSI. On the other hand, all macrozones show an increase in the
 297 trend in all the drought indices, with “Norte Grande” having the highest at 36 months (0.042 per decade).
 298 Because of this, the SPEI (which uses AED) reached its lowest value in “Norte Grande,” with -0.03 at 36
 299 months. Despite the other macrozones, “Austral” showed an increase in all indices, being the highest for
 300 EDDI at 36 months (0.025) and the lowest for SSI, which shows only a minor increase in the trend (Figure 5
 301 and Figure 4).

302 4.4. Impact for water supply and demand, and soil moisture in vegetation productivity

303 According to what is shown in Figure 6, Figure 7, and Table 4, forest seems to be the most resistant type
 304 to drought. Showing that only “Centro” is slightly ($rsq = 0.25$) impacted by a 12-month soil moisture deficit
 305 (SSI-12). In the “Norte Chico” and to a lesser extent in the “Norte Grande,” it is evident that a SSI-12 with
 306 a $rsq = 0.45$ and a decrease in water supply (SPI-36 and SPEI-24 with $rsq = 0.28$ and 0.34, respectively)
 307 have an impact on grasslands. However, this type was unaffected by soil moisture, water supply, or demand
 308 in macrozones further south. The types that show to be most affected by variation in climate conditions
 309 are shrublands, savannas, and croplands. For savannas in “Norte Chico,” the SSI-12 and SPI-24 reached
 310 an rsq of 0.74 and 0.58, respectively. This value decreases to the south, but the SSI-12 is still the variable
 311 explaining more of the variation in vegetation productivity ($rsq = 0.45$ in “Centro” and 0.2 in “Sur”). In
 312 the case of croplands, the SPEI-12, SPI-36, and SSI-12 explain between 45% and 66% of “Norte Chico.”
 313 The type of land most impacted by climatic variation was shrubland, where soil moisture explained 59%
 314 and precipitation, 37%, in “Norte Chico” and “Centro,” with SSI-12 being the most relevant variable, then
 315 SPI-36 in “Norte Chico” and SPI-24 in “Sur.”

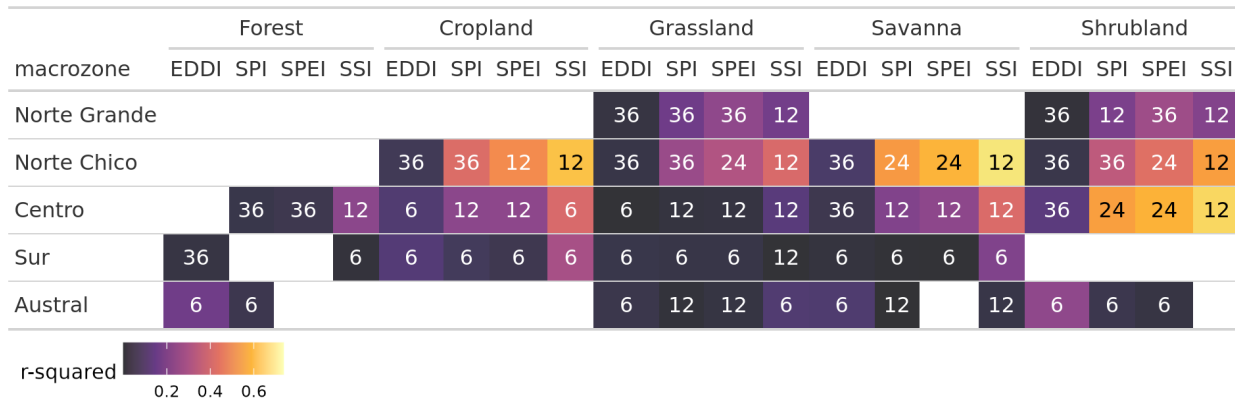


(c) EDDI (Evaporative Demand Drought Index)

(d) SSMI (Standardized Soil Moisture Index)

Figure 5: Linear trend of the drought index (*) at time scales of 1, 3, 6, 12, 24, and 36 months for 1981-2023

Table 4: Summary per land cover macroclass and macrozone regarding the correlation between zcNDVI with the drought indices EDDI, SPI, SPEI, and SSI for time scales of 1, 3, 6, 12, 24, and 36. The numbers in each cell indicate the time scale that reached the maximum correlation for the land cover and macrozone, and the color indicates the strength of the r-squared obtained with the index and the time scale.



316 5. Discussion

317 5.1. Ecological and agricultural drought

318 5.2. Drought trend, LULCC, and climate conditions

319 1.- Respecto a lo que indica [Vicente-Serrano et al. \(2018\)](#), de que el aumento en la tendencia en severidad
 320 de la sequía (hidrológica) tiene que ver más con un aumento de la demanda de agua (ej, LULCC, amazonas)
 321 que a una tendencia en las condiciones climáticas (SPI-12). ¿Qué pasa en Chile?

322 5.3. land cover types most impacted by drought throughout Chile

323 2.- Sobre los tipos de land cover más afectados por los indicadores de sequía. Asociación con el matorral
 324 chileno ([Fuentes et al., 2021](#)). Diferencia entre el Norte Chico, Centro y lo que pasa hacia el sur.

325 5.4. Drought indices of water demand and supply, soil moisture to predict changes in vegetation productivity

326 3. Como podrían servir estos resultados para desarrollar o mejorar un predictor de productividad de la
 327 vegetación.

- 328 • Los datos ERA5L están casi en tiempo real, 7 días; MODIS también.
- 329 • EL SSI se ve como un poderoso indicador que explica la variabilidad en la productividad de la veg-
 330 etación.

331 5.5. Future outlook

332 4.- Qué se podría hacer mejor en futuras investigaciones del tema. - mejorar la resolución y calidad de los
 333 datos climáticos -

334 6. Conclusion

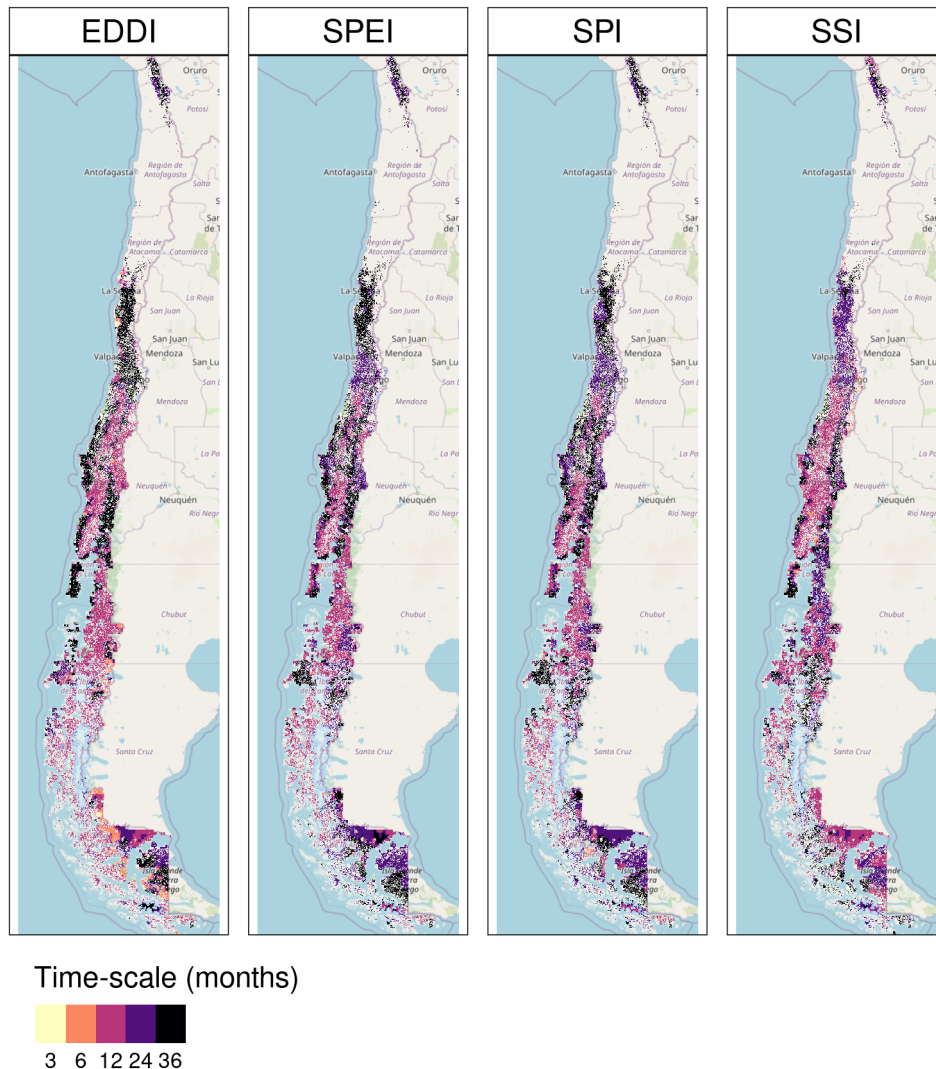


Figure 6: Time scales per drought index that reach the maximum coefficient of determination

References

- 335 Abramowitz, M., Stegun, I.A., 1968. Handbook of mathematical functions with formulas, graphs, and mathematical tables. 336 volume 55. US Government printing office.
- 337 Aceituno, P., Boisier, J.P., Garreaud, R., Rondanelli, R., Rulltall, J.A., 2021. Climate and Weather in Chile, in: Fernández, 338 B., Gironás, J. (Eds.), Water Resources of Chile. Springer International Publishing, Cham. volume 8, pp. 7–29. URL: 339 http://link.springer.com/10.1007/978-3-030-56901-3_2.
- 340 AghaKouchak, A., 2014. A baseline probabilistic drought forecasting framework using standardized soil moisture index: 341 application to the 2012 United States drought. Hydrology and Earth System Sciences 18, 2485–2492. URL: 342 <https://hess.copernicus.org/articles/18/2485/2014/>, doi:[10.5194/hess-18-2485-2014](https://doi.org/10.5194/hess-18-2485-2014).
- 343 AghaKouchak, A., Farahmand, A., Melton, F.S., Teixeira, J., Anderson, M.C., Wardlow, B.D., Hain, C.R., 2015. Remote 344 sensing of drought: Progress, challenges and opportunities. Reviews of Geophysics 53, 452–480. URL: <http://dx.doi.org/10.1002/2014RG000456>, doi:[10.1002/2014RG000456](https://doi.org/10.1002/2014RG000456).
- 345 AghaKouchak, A., Mirchi, A., Madani, K., Di Baldassarre, G., Nazemi, A., Alborzi, A., Anjileli, H., Azarderakhsh, M., Chiang, 346 F., Hassanzadeh, E., Huning, L.S., Mallakpour, I., Martinez, A., Mazdiyasni, O., Moftakhar, H., Norouzi, H., Sadegh, 347 M., Sadeqi, D., Van Loon, A.F., Wanders, N., 2021. Anthropogenic Drought: Definition, Challenges, and Opportunities. 348 Reviews of Geophysics 59, e2019RG000683. URL: <https://agupubs.onlinelibrary.wiley.com/doi/10.1029/2019RG000683>, doi:[10.1029/2019RG000683](https://doi.org/10.1029/2019RG000683).
- 349 Ahmed, M., Sultan, M., Wahr, J., Yan, E., 2014. The use of GRACE data to monitor natural and anthropogenic induced 350
- 351
- 352

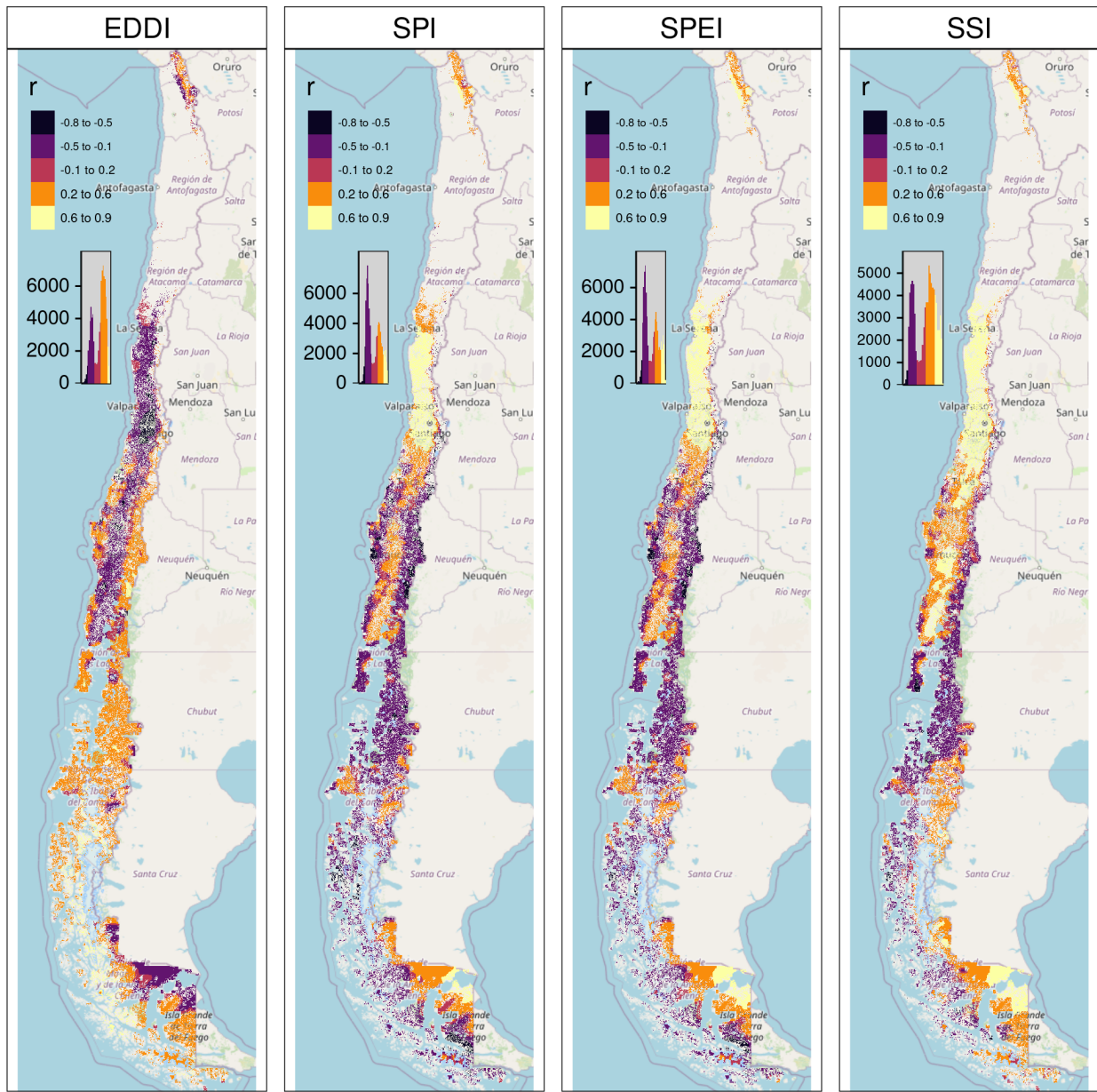


Figure 7: Pearson correlation value for the time scales and drought index that reach the maximum coefficient of determination

- variations in water availability across Africa. *Earth-Science Reviews* 136, 289–300. doi:[10.1016/J.EARSCIREV.2014.05.009](https://doi.org/10.1016/J.EARSCIREV.2014.05.009). publisher: Elsevier.
- Akinyemi, F.O., 2021. Vegetation Trends, Drought Severity and Land Use-Land Cover Change during the Growing Season in Semi-Arid Contexts. *Remote Sensing* 2021, Vol. 13, Page 836 13, 836. URL: <https://www.mdpi.com/2072-4292/13/5/836/>, doi:[10.3390/RS13050836](https://doi.org/10.3390/RS13050836). publisher: Multidisciplinary Digital Publishing Institute.
- Alvarez-Garreton, C., Boisier, J.P., Garreaud, R., Seibert, J., Vis, M., 2021. Progressive water deficits during multiyear droughts in basins with long hydrological memory in Chile. *Hydrology and Earth System Sciences* 25, 429–446. URL: <https://hess.copernicus.org/articles/25/429/2021/>, doi:[10.5194/hess-25-429-2021](https://doi.org/10.5194/hess-25-429-2021).
- Beck, H.E., McVicar, T.R., Vergopolan, N., Berg, A., Lutsko, N.J., Dufour, A., Zeng, Z., Jiang, X., van Dijk, A.I.J.M., Miralles, D.G., 2023. High-resolution (1 km) Köppen-Geiger maps for 1901–2099 based on constrained CMIP6 projections. *Scientific Data* 10. URL: <http://dx.doi.org/10.1038/s41597-023-02549-6>, doi:[10.1038/s41597-023-02549-6](https://doi.org/10.1038/s41597-023-02549-6).
- Beguería, S., Vicente-Serrano, S.M., 2023. SPEI: Calculation of the Standardized Precipitation-Evapotranspiration Index. URL:

- 365 <https://CRAN.R-project.org/package=SPEI>.
- 366 Boisier, J.P., Alvarez-Garreton, C., Cordero, R.R., Damiani, A., Gallardo, L., Garreaud, R.D., Lambert, F., Ramallo, C.,
 367 Rojas, M., Rondanelli, R., 2018. Anthropogenic drying in central-southern Chile evidenced by long-term observations
 368 and climate model simulations. *Elementa* 6, 74. URL: <https://www.elementascience.org/article/10.1525/elementa.328/>,
 369 doi:[10.1525/elementa.328](https://doi.org/10.1525/elementa.328).
- 370 Calvin, K., Dasgupta, D., Krinner, G., Mukherji, A., Thorne, P.W., Trisos, C., Romero, J., Aldunce, P., Barrett, K., Blanco,
 371 G., Cheung, W.W., Connors, S., Denton, F., Diongue-Niang, A., Dodman, D., Garschagen, M., Geden, O., Hayward, B.,
 372 Jones, C., Jotzo, F., Krug, T., Lasco, R., Lee, Y.Y., Masson-Delmotte, V., Meinshausen, M., Mintenbeck, K., Mokssit, A.,
 373 Otto, F.E., Pathak, M., Pirani, A., Poloczanska, E., Pörtner, H.O., Revi, A., Roberts, D.C., Roy, J., Ruane, A.C., Skea,
 374 J., Shukla, P.R., Slade, R., Slangen, A., Sokona, Y., Sörensson, A.A., Tignor, M., Van Vuuren, D., Wei, Y.M., Winkler,
 375 H., Zhai, P., Zommers, Z., Hourcade, J.C., Johnson, F.X., Pachauri, S., Simpson, N.P., Singh, C., Thomas, A., Totin, E.,
 376 Arias, P., Bustamante, M., Elgizouli, I., Flato, G., Howden, M., Méndez-Vallejo, C., Pereira, J.J., Pichs-Madruga, R., Rose,
 377 S.K., Saheb, Y., Sánchez Rodríguez, R., Ürge Vorsatz, D., Xiao, C., Yassaai, N., Alegría, A., Armour, K., Bednar-Friedl, B.,
 378 Blok, K., Cissé, G., Dentener, F., Eriksen, S., Fischer, E., Garner, G., Guivarc, C., Haasnoot, M., Hansen, G., Hauser, M.,
 379 Hawkins, E., Hermans, T., Kopp, R., Leprince-Ringuet, N., Lewis, J., Ley, D., Ludden, C., Niamir, L., Nicholls, Z., Some,
 380 S., Szopa, S., Trewhin, B., Van Der Wijst, K.I., Winter, G., Witting, M., Birt, A., Ha, M., Romero, J., Kim, J., Haites, E.F.,
 381 Jung, Y., Stavins, R., Birt, A., Ha, M., Orendain, D.J.A., Ignon, L., Park, S., Park, Y., Reisinger, A., Cammaramo, D.,
 382 Fischlin, A., Fuglestvedt, J.S., Hansen, G., Ludden, C., Masson-Delmotte, V., Matthews, J.R., Mintenbeck, K., Pirani, A.,
 383 Poloczanska, E., Leprince-Ringuet, N., Péan, C., 2023. IPCC, 2023: Climate Change 2023: Synthesis Report. Contribution
 384 of Working Groups I, II and III to the Sixth Assessment Report of the Intergovernmental Panel on Climate Change [Core
 385 Writing Team, H. Lee and J. Romero (eds.)]. IPCC, Geneva, Switzerland. Technical Report. Intergovernmental Panel on
 386 Climate Change (IPCC). URL: <https://www.ipcc.ch/report/ar6/syr/>.
- 387 Crausbay, S.D., Ramirez, A.R., Carter, S.L., Cross, M.S., Hall, K.R., Bathke, D.J., Betancourt, J.L., Colt, S., Cravens, A.E.,
 388 Dalton, M.S., Dunham, J.B., Hay, L.E., Hayes, M.J., McEvoy, J., McNutt, C.A., Moritz, M.A., Nislow, K.H., Raheem, N.,
 389 Sanford, T., 2017. Defining Ecological Drought for the Twenty-First Century. *Bulletin of the American Meteorological Society*
 390 98, 2543–2550. URL: <https://journals.ametsoc.org/view/journals/bams/98/12/bams-d-16-0292.1.xml>, doi:[10.1175/BAMS-D-16-0292.1](https://doi.org/10.1175/BAMS-D-16-0292.1). publisher: American Meteorological Society.
- 391 Cui, A., Li, J., Zhou, Q., Zhu, R., Liu, H., Wu, G., Li, Q., 2021. Use of a multiscalar GRACE-based standardized terrestrial
 392 water storage index for assessing global hydrological droughts. *Journal of Hydrology* 603, 126871. URL: <https://linkinghub.elsevier.com/retrieve/pii/S0022169421009215>, doi:[10.1016/j.jhydrol.2021.126871](https://doi.org/10.1016/j.jhydrol.2021.126871).
- 392 Didan, K., 2015. MOD13Q1 MODIS/Terra Vegetation Indices 16-Day L3 Global 250m SIN Grid V006. Technical Report.
 393 NASA EOSDIS Land Processes DAAC. doi:<http://dx.doi.org/10.5067/MODIS/MOD13Q1.006>.
- 394 Fernández, F.J., Vásquez-Lavín, F., Ponce, R.D., Garreaud, R., Hernández, F., Link, O., Zambrano, F., Hanemann, M., 2023.
 395 The economics impacts of long-run droughts: Challenges, gaps, and way forward. *Journal of Environmental Management*
 396 344, 118726. URL: <https://linkinghub.elsevier.com/retrieve/pii/S0301479723015141>, doi:[10.1016/j.jenvman.2023.118726](https://doi.org/10.1016/j.jenvman.2023.118726).
- 397 Friedl, M., Sulla-Menashe, D., 2019. MCD12Q1 MODIS/Terra+Aqua Land Cover Type Yearly L3 Global 500m SIN Grid V006
 398 [Data set]. NASA EOSDIS Land Processes DAAC. doi:[10.5067/MODIS/MCD12Q1.006](http://dx.doi.org/10.5067/MODIS/MCD12Q1.006).
- 399 Fuentes, I., Fuster, R., Avilés, D., Vervoort, W., 2021. Water scarcity in central Chile: the effect of climate and land cover
 400 changes on hydrologic resources. *Hydrological Sciences Journal* 66, 1028–1044. URL: <https://www.tandfonline.com/doi/full/10.1080/02626667.2021.1903475>, doi:[10.1080/02626667.2021.1903475](https://doi.org/10.1080/02626667.2021.1903475).
- 401 Garreaud, R., Alvarez-Garreton, C., Barichivich, J., Boisier, J.P., Christie, D., Galleguillos, M., LeQuenne, C., McPhee, J.,
 402 Zambrano-Bigiarini, M., 2017. The 2010–2015 mega drought in Central Chile: Impacts on regional hydroclimate and
 403 vegetation. *Hydrology and Earth System Sciences Discussions* 2017, 1–37. URL: <http://www.hydrol-earth-syst-sci-discuss.net/hess-2017-191/>, doi:[10.5194/hess-2017-191](https://doi.org/10.5194/hess-2017-191).
- 404 Garreaud, R.D., 2009. The Andes climate and weather. *Advances in Geosciences* 22, 3–11. URL: <https://adgeo.copernicus.org/articles/22/3/2009/>, doi:[10.5194/adgeo-22-3-2009](https://doi.org/10.5194/adgeo-22-3-2009).
- 405 Garreaud, R.D., Boisier, J.P., Rondanelli, R., Montecinos, A., Sepúlveda, H.H., Veloso-Aguila, D., 2020. The Central Chile
 406 Mega Drought (2010–2018): A climate dynamics perspective. *International Journal of Climatology* 40, 421–439. URL:
 407 <https://rmets.onlinelibrary.wiley.com/doi/10.1002/joc.6219>, doi:[10.1002/joc.6219](https://doi.org/10.1002/joc.6219).
- 408 Grekousis, G., Mountrakis, G., Kavouras, M., 2015. An overview of 21 global and 43 regional land-cover mapping products.
 409 *International Journal of Remote Sensing* 36, 5309–5335. URL: <https://www.tandfonline.com/doi/full/10.1080/01431161.2015.1093195>, doi:[10.1080/01431161.2015.1093195](https://doi.org/10.1080/01431161.2015.1093195).
- 410 Hao, Z., AghaKouchak, A., 2013. Multivariate Standardized Drought Index: A parametric multi-index model. *Advances in Water
 411 Resources* 57, 12–18. URL: <https://linkinghub.elsevier.com/retrieve/pii/S0309170813000493>, doi:[10.1016/j.advwatres.2013.03.009](https://doi.org/10.1016/j.advwatres.2013.03.009).
- 412 Hargreaves, G.H., 1994. Defining and Using Reference Evapotranspiration. *Journal of Irrigation and Drainage Engineering* 120,
 413 1132–1139. URL: <https://ascelibrary.org/doi/10.1061/%28ASCE%290733-9437%281994%29120%3A6%281132%29>, doi:[10.1061/\(ASCE\)0733-9437\(1994\)120:6\(1132\)](https://doi.org/10.1061/(ASCE)0733-9437(1994)120:6(1132)).
- 414 Hargreaves, G.H., Samani, Z.A., 1985. Reference crop evapotranspiration from temperature. *Applied engineering in agriculture*
 415 1, 96–99.
- 416 Hijmans, R.J., 2023. terra: Spatial Data Analysis. URL: <https://CRAN.R-project.org/package=terra>.
- 417 Ho, T.K., 1995. Random decision forests, in: *Proceedings of 3rd international conference on document analysis and recognition*,
 418 IEEE. pp. 278–282.
- 419 Hobbins, M.T., Wood, A., McEvoy, D.J., Huntington, J.L., Morton, C., Anderson, M., Hain, C., 2016. The Evaporative Demand
 420 Drought Index. Part I: Linking Drought Evolution to Variations in Evaporative Demand. *Journal of Hydrometeorology* 17,

- 430 1745–1761. URL: <http://journals.ametsoc.org/doi/10.1175/JHM-D-15-0121.1>, doi:[10.1175/JHM-D-15-0121.1](https://doi.org/10.1175/JHM-D-15-0121.1).
- 431 Hoerl, A.E., Kennard, R.W., 1970. Ridge Regression: Biased Estimation for Nonorthogonal Problems. *Technometrics* 12, 55–67.
- 432 URL: <http://www.tandfonline.com/doi/abs/10.1080/00401706.1970.10488634>, doi:[10.1080/00401706.1970.10488634](https://doi.org/10.1080/00401706.1970.10488634).
- 433 Hufkens, K., Stauffer, R., Campitelli, E., 2019. The ecwmfr package: an interface to ECMWF API endpoints. URL: <https://bluegreen-labs.github.io/ecmwfr/>.
- 434 IPCC, 2013. Climate Change 2013: The Physical Science Basis. Contribution of Working Group I to the Fifth Assessment Report of the Intergovernmental Panel on Climate Change. Cambridge University Press, Cambridge, UK; New York, USA.
- 435 URL: www.climatechange2013.org, doi:[10.1017/CBO9781107415324](https://doi.org/10.1017/CBO9781107415324).
- 436 Kendall, M., 1975. Rank correlation methods (4th ed. 2d impression). Griffin.
- 437 Kogan, F.N., 1995. Application of vegetation index and brightness temperature for drought detection. *Advances in Space Research* 15, 91–100. doi:[10.1016/0273-1177\(95\)00079-T](https://doi.org/10.1016/0273-1177(95)00079-T).
- 438 Luo, L., Apps, D., Arcand, S., Xu, H., Pan, M., Hoerling, M., 2017. Contribution of temperature and precipitation anomalies to the California drought during 2012–2015. *Geophysical Research Letters* 44, 3184–3192. URL: <https://agupubs.onlinelibrary.wiley.com/doi/10.1002/2016GL072027>, doi:[10.1002/2016GL072027](https://doi.org/10.1002/2016GL072027).
- 439 Ma, S., Wu, Q., Wang, J., Zhang, S., 2017. Temporal Evolution of Regional Drought Detected from GRACE TWSA and CCI SM in Yunnan Province, China. *Remote Sensing* 2017, Vol. 9, Page 1124 9, 1124. URL: <https://www.mdpi.com/2072-4292/9/11/1124/htm>, doi:[10.3390/RS9111124](https://doi.org/10.3390/RS9111124). publisher: Multidisciplinary Digital Publishing Institute.
- 440 McEvoy, D.J., Huntington, J.L., Hobbins, M.T., Wood, A., Morton, C., Anderson, M., Hain, C., 2016. The Evaporative Demand Drought Index. Part II: CONUS-Wide Assessment against Common Drought Indicators. *Journal of Hydrometeorology* 17, 1763–1779. URL: <http://journals.ametsoc.org/doi/10.1175/JHM-D-15-0122.1>, doi:[10.1175/JHM-D-15-0122.1](https://doi.org/10.1175/JHM-D-15-0122.1).
- 441 McKee, T.B., Doesken, N.J., Kleist, J., 1993. The relationship of drought frequency and duration to time scales. In: Proceedings of the Ninth Conference on Applied Climatology. American Meteorological Society , 179–184.
- 442 Meroni, M., Rembold, F., Fasbender, D., Vrieling, A., 2017. Evaluation of the Standardized Precipitation Index as an early predictor of seasonal vegetation production anomalies in the Sahel. *Remote Sensing Letters* 8, 301–310. URL: <https://www.tandfonline.com/doi/full/10.1080/2150704X.2016.1264020>, doi:[10.1080/2150704X.2016.1264020](https://doi.org/10.1080/2150704X.2016.1264020).
- 443 Miranda, A., Lara, A., Altamirano, A., Di Bella, C., González, M.E., Julio Camarero, J., 2020. Forest browning trends in response to drought in a highly threatened mediterranean landscape of South America. *Ecological Indicators* 115, 106401. URL: <https://linkinghub.elsevier.com/retrieve/pii/S1470160X20303381>, doi:[10.1016/j.ecolind.2020.106401](https://doi.org/10.1016/j.ecolind.2020.106401).
- 444 Miranda, A., Syphard, A.D., Berdugo, M., Carrasco, J., Gómez-González, S., Ovalle, J.F., Delpiano, C.A., Vargas, S., Squeo, F.A., Miranda, M.D., Dobbs, C., Mentler, R., Lara, A., Garreaud, R., 2023. Widespread synchronous decline of Mediterranean-type forest driven by accelerated aridity. *Nature Plants* 9, 1810–1817. URL: <https://www.nature.com/articles/s41477-023-01541-7>, doi:[10.1038/s41477-023-01541-7](https://doi.org/10.1038/s41477-023-01541-7).
- 445 Muñoz-Sabater, J., Dutra, E., Agustí-Panareda, A., Albergel, C., Arduini, G., Balsamo, G., Boussetta, S., Choulga, M., Harrigan, S., Hersbach, H., Martens, B., Miralles, D.G., Piles, M., Rodríguez-Fernández, N.J., Zsoter, E., Buontempo, C., Thépaut, J.N., 2021. ERA5-Land: a state-of-the-art global reanalysis dataset for land applications. *Earth System Science Data* 13, 4349–4383. URL: <https://essd.copernicus.org/articles/13/4349/2021/>, doi:[10.5194/essd-13-4349-2021](https://doi.org/10.5194/essd-13-4349-2021).
- 446 Narasimhan, B., Srinivasan, R., 2005. Development and evaluation of Soil Moisture Deficit Index (SMDI) and Evapotranspiration Deficit Index (ETDI) for agricultural drought monitoring. *Agricultural and Forest Meteorology* 133, 69–88. URL: <https://linkinghub.elsevier.com/retrieve/pii/S0168192305001565>, doi:[10.1016/j.agrformet.2005.07.012](https://doi.org/10.1016/j.agrformet.2005.07.012).
- 447 Nouri, M., 2023. Drought Assessment Using Gridded Data Sources in Data-Poor Areas with Different Aridity Conditions. *Water Resources Management* 37, 4327–4343. URL: <https://link.springer.com/10.1007/s11269-023-03555-4>, doi:[10.1007/s11269-023-03555-4](https://doi.org/10.1007/s11269-023-03555-4).
- 448 Paruelo, J.M., Texeira, M., Staiano, L., Mastrángelo, M., Amdan, L., Gallego, F., 2016. An integrative index of Ecosystem Services provision based on remotely sensed data. *Ecological Indicators* 71, 145–154. URL: <https://www.sciencedirect.com/science/article/pii/S1470160X16303843>, doi:[10.1016/J.ECOLIND.2016.06.054](https://doi.org/10.1016/J.ECOLIND.2016.06.054). publisher: Elsevier.
- 449 Pebesma, E., 2018. Simple Features for R: Standardized Support for Spatial Vector Data. *The R Journal* 10, 439–446. URL: <https://doi.org/10.32614/RJ-2018-009>, doi:[10.32614/RJ-2018-009](https://doi.org/10.32614/RJ-2018-009).
- 450 Pebesma, E., Bivand, R., 2023. Spatial Data Science: With applications in R. Chapman and Hall/CRC, London. URL: <https://r-spatial.org/book/>.
- 451 R Core Team, 2023. R: A Language and Environment for Statistical Computing. R Foundation for Statistical Computing, Vienna, Austria. URL: <https://www.R-project.org/>.
- 452 Schucknecht, A., Meroni, M., Kayitakire, F., Boureima, A., Schucknecht, A., Meroni, M., Kayitakire, F., Boureima, A., 2017. Phenology-Based Biomass Estimation to Support Rangeland Management in Semi-Arid Environments. *Remote Sensing* 9, 463. URL: <https://www.mdpi.com/2072-4292/9/5/463>, doi:[10.3390/rs9050463](https://doi.org/10.3390/rs9050463). publisher: Multidisciplinary Digital Publishing Institute.
- 453 Sen, P.K., 1968. Estimates of the Regression Coefficient Based on Kendall's Tau. *Journal of the American Statistical Association* 63, 1379–1389. URL: <http://www.tandfonline.com/doi/abs/10.1080/01621459.1968.10480934>, doi:[10.1080/01621459.1968.10480934](https://doi.org/10.1080/01621459.1968.10480934).
- 454 Seneviratne, S and Zhang, X.a.A.M.a.B.W.a.D.C.a.L.A.a.G.S.a.I.I.a.K.J.a.L.S.a.O.F.a.P.I.a.S.M.a.V.S.S.a.W.M.a.Z..M.D.B.a.V.a.O., 2021. Weather and Climate Extreme Events in a Changing Climate. Cambridge University Press. In Press. Publication Title: Climate Change 2021: The Physical Science Basis. Contribution of Working Group I to the Sixth Assessment Report of the Intergovernmental Panel on Climate Change.
- 455 Slette, I.J., Post, A.K., Awad, M., Even, T., Punzalan, A., Williams, S., Smith, M.D., Knapp, A.K., 2019. How ecologists define drought, and why we should do better. *Global Change Biology* 25, 3193–3200. URL: <https://onlinelibrary.wiley.com/doi/10.1111/gcb.14747>, doi:[10.1111/gcb.14747](https://doi.org/10.1111/gcb.14747).

- 495 Souza, A.G.S.S., Ribeiro Neto, A., Souza, L.L.D., 2021. Soil moisture-based index for agricultural drought assessment: SMADI
 496 application in Pernambuco State-Brazil. *Remote Sensing of Environment* 252, 112124. URL: <https://linkinghub.elsevier.com/retrieve/pii/S0034425720304971>, doi:[10.1016/j.rse.2020.112124](https://doi.org/10.1016/j.rse.2020.112124).
- 497 Tibshirani, R., Bien, J., Friedman, J., Hastie, T., Simon, N., Taylor, J., Tibshirani, R.J., 2010. Strong rules for discarding
 498 predictors in lasso-type problems. URL: <http://arxiv.org/abs/1011.2234>.
- 499 Tran, H.T., Campbell, J.B., Wynne, R.H., Shao, Y., Phan, S.V., 2019. Drought and Human Impacts on Land Use and Land
 500 Cover Change in a Vietnamese Coastal Area. *Remote Sensing* 2019, Vol. 11, Page 333 11, 333. URL: <https://www.mdpi.com/2072-4292/11/3/333/htm>, doi:[10.3390/RS11030333](https://doi.org/10.3390/RS11030333). publisher: Multidisciplinary Digital Publishing Institute.
- 501 Urrutia-Jalabert, R., González, M.E., González-Reyes, ., Lara, A., Garreaud, R., 2018. Climate variability and forest fires in
 502 central and south-central Chile. *Ecosphere* 9, e02171. URL: <https://esajournals.onlinelibrary.wiley.com/doi/10.1002/ecs2.2171>, doi:[10.1002/ecs2.2171](https://doi.org/10.1002/ecs2.2171).
- 503 Van Loon, A.F., Gleeson, T., Clark, J., Van Dijk, A.I., Stahl, K., Hannaford, J., Di Baldassarre, G., Teuling, A.J., Tallaksen,
 504 L.M., Uijlenhoet, R., Hannah, D.M., Sheffield, J., Svoboda, M., Verbeiren, B., Wagener, T., Rangecroft, S., Wanders, N.,
 505 Van Lanen, H.A., 2016. Drought in the Anthropocene. *Nature Geoscience* 9, 89–91. doi:[10.1038/ngeo2646](https://doi.org/10.1038/ngeo2646).
- 506 Venegas-González, A., Juñent, F.R., Gutiérrez, A.G., Filho, M.T., 2018. Recent radial growth decline in response to increased
 507 drought conditions in the northernmost Nothofagus populations from South America. *Forest Ecology and Management* 409,
 508 94–104. URL: <https://linkinghub.elsevier.com/retrieve/pii/S0378112717313993>, doi:[10.1016/j.foreco.2017.11.006](https://doi.org/10.1016/j.foreco.2017.11.006).
- 509 Vicente-Serrano, S.M., Azorin-Molina, C., Sanchez-Lorenzo, A., Revuelto, J., López-Moreno, J.I., González-Hidalgo, J.C.,
 510 Moran-Tejeda, E., Espejo, F., 2014. Reference evapotranspiration variability and trends in Spain, 1961–2011. *Global
 511 and Planetary Change* 121, 26–40. URL: <https://linkinghub.elsevier.com/retrieve/pii/S0921818114001180>, doi:[10.1016/j.gloplacha.2014.06.005](https://doi.org/10.1016/j.gloplacha.2014.06.005).
- 512 Vicente-Serrano, S.M., Beguería, S., López-Moreno, J.I., 2010. A multiscalar drought index sensitive to global warming: The
 513 standardized precipitation evapotranspiration index. *Journal of Climate* 23, 1696–1718. URL: <http://dx.doi.org/10.1175/2009JCLI2909.1>, doi:[10.1175/2009JCLI2909.1](https://doi.org/10.1175/2009JCLI2909.1).
- 514 Vicente-Serrano, S.M., Miralles, D.G., Domínguez-Castro, F., Azorin-Molina, C., El Kenawy, A., McVicar, T.R., Tomás-
 515 Burguera, M., Beguería, S., Maneta, M., Peña-Gallardo, M., 2018. Global Assessment of the Standardized Evapotranspiration
 516 Deficit Index (SEDI) for Drought Analysis and Monitoring. *Journal of Climate* 31, 5371–5393. URL: <https://journals.ametsoc.org/doi/10.1175/JCLI-D-17-0775.1>, doi:[10.1175/JCLI-D-17-0775.1](https://doi.org/10.1175/JCLI-D-17-0775.1).
- 517 Vicente-Serrano, S.M., Peña-Angulo, D., Beguería, S., Domínguez-Castro, F., Tomás-Burguera, M., Noguera, I., Gimeno-Sotelo,
 518 L., El Kenawy, A., 2022. Global drought trends and future projections. *Philosophical Transactions of the Royal Society A: Mathematical, Physical and Engineering Sciences* 380, 20210285. URL: <https://royalsocietypublishing.org/doi/10.1098/rsta.2021.0285>, doi:[10.1098/rsta.2021.0285](https://doi.org/10.1098/rsta.2021.0285).
- 519 Wang, M., Menzel, L., Jiang, S., Ren, L., Xu, C.Y., Cui, H., 2023. Evaluation of flash drought under the impact of heat wave
 520 events in southwestern Germany. *Science of The Total Environment* 904, 166815. URL: <https://linkinghub.elsevier.com/retrieve/pii/S0048969723054402>, doi:[10.1016/j.scitotenv.2023.166815](https://doi.org/10.1016/j.scitotenv.2023.166815).
- 521 West, H., Quinn, N., Horswell, M., 2019. Remote sensing for drought monitoring \& impact assessment: Progress, past
 522 challenges and future opportunities. *Remote Sensing of Environment* 232. doi:[10.1016/j.rse.2019.111291](https://doi.org/10.1016/j.rse.2019.111291). publisher:
 523 Elsevier Inc.
- 524 Wilhite, D.A., Glantz, M.H., 1985. Understanding: The drought phenomenon: The role of definitions. *Water International* 10,
 525 111–120. URL: <http://dx.doi.org/10.1080/02508068508686328>, doi:[10.1080/02508068508686328](https://doi.org/10.1080/02508068508686328).
- 526 Wilks, D.S., 2011. Empirical distributions and exploratory data analysis. *Statistical Methods in the Atmospheric Sciences* 100.
- 527 WMO, Svoboda, M., Hayes, M., Wood, D.A., 2012. Standardized Precipitation Index User Guide. WMO, Geneva. URL:
 528 http://library.wmo.int/opac/index.php?lvl=notice_display&id=13682. series Title: WMO Publication Title: WMO-No.
 529 1090 © Issue: 1090.
- 530 Zambrano, F., 2023. Four decades of satellite data for agricultural drought monitoring throughout the growing season in Central
 531 Chile, in: Vijay P. Singh Deepak Jhajharia, R.M., Kumar, R. (Eds.), *Integrated Drought Management*, Two Volume Set.
 532 CRC Press, p. 28.
- 533 Zambrano, F., Lillo-Saavedra, M., Verbist, K., Lagos, O., 2016. Sixteen years of agricultural drought assessment of the
 534 biobío region in chile using a 250 m resolution vegetation condition index (VCI). *Remote Sensing* 8, 1–20. URL: <https://www.mdpi.com/2072-4292/8/6/530>, doi:[10.3390/rs8060530](https://doi.org/10.3390/rs8060530). publisher: Multidisciplinary Digital Publishing Institute.
- 535 Zambrano, F., Vrieling, A., Nelson, A., Meroni, M., Tadesse, T., 2018. Prediction of drought-induced reduction of agricultural
 536 productivity in Chile from MODIS, rainfall estimates, and climate oscillation indices. *Remote Sensing of Environment*
 537 219, 15–30. URL: <https://www.sciencedirect.com/science/article/pii/S0034425718304541>, doi:[10.1016/j.rse.2018.10.006](https://doi.org/10.1016/j.rse.2018.10.006).
 538 publisher: Elsevier.
- 539 Zhao, Y., Feng, D., Yu, L., Wang, X., Chen, Y., Bai, Y., Hernández, H.J., Galleguillos, M., Estades, C., Biging, G.S., Radke,
 540 J.D., Gong, P., 2016. Detailed dynamic land cover mapping of Chile: Accuracy improvement by integrating multi-temporal
 541 data. *Remote Sensing of Environment* 183, 170–185. URL: <https://linkinghub.elsevier.com/retrieve/pii/S0034425716302188>,
 542 doi:[10.1016/j.rse.2016.05.016](https://doi.org/10.1016/j.rse.2016.05.016).